European Journal of Cell Biology 98 (2019) 12–26

Contents lists available at ScienceDirect

European Journal of Cell Biology

journal homepage: www.elsevier.com/locate/ejcb

Research paper

WDR20 regulates shuttling of the USP12 deubiquitinase complex between the plasma membrane, cytoplasm and nucleus

Anne Olazabal-Herrero[a], Maria Sendino[a], Ignacio Arganda-Carreras[b,c,d], Jose Antonio Rodríguez[a,*]

[a] Department of Genetics, Physical Anthropology and Animal Physiology, University of the Basque Country (UPV/EHU), Leioa 48940, Spain
[b] Computer Science and Artificial Intelligence Department, University of the Basque Country (UPV/EHU), San Sebastian 20018, Spain
[c] Ikerbasque, Basque Foundation for Science, Maria Diaz de Haro 3, 48013 Bilbao, Spain
[d] Donostia International Physics Center (DIPC), P. Manuel Lardizabal 4, 20018 San Sebastian, Spain

ARTICLE INFO

Keywords:
Deubiquitinase
USP12
USP46
WDR20
UAF1
CRM1

ABSTRACT

The human deubiquitinases USP12 and USP46 are very closely related paralogs with critical functions as tumor suppressors. The catalytic activity of these enzymes is regulated by two cofactors: UAF1 and WDR20. USP12 and USP46 show nearly 90% amino acid sequence identity and share some cellular activities, but have also evolved non-overlapping functions. We hypothesized that, correlating with their functional divergence, the subcellular localization of USP12 and USP46 might be differentially regulated by their cofactors. We used confocal and live microscopy analyses of epitope-tagged proteins to determine the effect of UAF1 and WDR20 on the localization of USP12 and USP46. We found that WDR20 differently modulated the localization of the DUBs, promoting recruitment of USP12, but not USP46, to the plasma membrane. Using site-directed mutagenesis, we generated a large set of USP12 and WDR20 mutants to characterize in detail the mechanisms and sequence determinants that modulate the subcellular localization of the USP12/UAF1/WDR20 complex. Our data suggest that the USP12/UAF1/WDR20 complex dynamically shuttles between the plasma membrane, cytoplasm and nucleus. This shuttling involved active nuclear export mediated by the CRM1 pathway, and required a short N-terminal motif (^{1}MEIL^{4}) in USP12, as well as a novel nuclear export sequence (^{450}MDGAIASGVSKFATLSLHD^{468}) in WDR20. In conclusion, USP12 and USP46 have evolved divergently in terms of cofactor binding-regulated subcellular localization. WDR20 plays a crucial role in as a "targeting subunit" that modulates CRM1-dependent shuttling of the USP12/UAF1/WDR20 complex between the plasma membrane, cytoplasm and nucleus.

1. Introduction

Ubiquitination is a reversible posttranslational modification that modulates stability, function and/or localization of most cellular proteins. Deubiquitinases (DUBs) are the enzymes that catalyze the removal of ubiquitin moieties from substrate proteins and thus, play a crucial role in many physiological processes (Komander et al., 2009). Functional alterations of several DUBs have been causally linked to tumor development, and some of these enzymes are increasingly regarded as promising targets in cancer therapy (Wei et al., 2015).

There are around 100 human DUBs, which can be classified in 7 families (Fraile et al., 2012; Haahr et al., 2018; Kwasna et al., 2018). The largest DUB family includes 54 enzymes termed ubiquitin-specific proteases (USPs), which share a structurally conserved catalytic domain (Ye et al., 2009). USP12 and USP46 are two members of the USP family that have critical functions as tumor suppressors (Gangula and Maddika, 2013; Li et al., 2013). Human USP12 and USP46 are very similar paralogs that show nearly 90% of amino acid sequence identity, and evolved from a single ancestor gene by a duplication event (Vlasschaert et al., 2017). Lower eukaryotes, such as the fission yeast *Schizosaccharomyces pombe* and invertebrates, such as a *Caenorhabditis elegans*, express a single DUB that is homologous to both USP12 and USP46.

Given their importance for the maintenance of cellular homeostasis,

Abbreviations: ActD, actinomycin D; CHX, cycloheximide; co-IP, co-immunoprecipitation; DUB, deubiquitinase; FRAP, fluorescence recovery after photobleaching; LMB, leptomycin B; NES, nuclear export sequence; NLS, nuclear localization signal; PHLPP, pleckstrin homology domain leucine rich repeat protein phosphatase; PM, plasma membrane; USP, ubiquitin-specific protease; WDR, WD40-repeat; YFP, yellow fluorescent protein

* Corresponding author.
E-mail address: josean.rodriguez@ehu.eus (J.A. Rodríguez).

https://doi.org/10.1016/j.ejcb.2018.10.003
Received 18 April 2018; Received in revised form 1 October 2018; Accepted 25 October 2018

the function of DUBs needs to be tightly regulated, and several mechanisms that modulate the activity of these enzymes have been described (reviewed in Mevissen and Komander, 2017). In the case of USP12 and USP46, the most critical regulatory event is their binding to the WD40-repeat (WDR) containing proteins UAF1 (also called WDR48) (Cohn et al., 2007; Cohn et al., 2009) and WDR20 (Kee et al., 2010; Dahlberg and Juo, 2014). These WDR proteins act synergistically as cofactors that dramatically increase the enzymatic activity of both USP12 and USP46 through a series of allosteric rearrangements in the DUB structure (Cohn et al., 2007, 2009; Kee et al., 2010; Dahlberg and Juo, 2014; Yin et al., 2015; Dharadhar et al., 2016; Li et al., 2016). This regulatory mechanism shows a remarkable evolutionary conservation, being already present in the fission yeast. Thus, the enzymatic activity of *S. pombe* Ubp9 (USP12 and USP46 homologue) is regulated by binding to Bun107 and Bun62, the yeast homologues of UAF1 and WDR20, respectively (Kouranti et al., 2010).

Despite their strikingly similar amino acid sequence, USP12 and USP46 exhibit a certain degree of functional divergence. Thus, although both DUBs participate in common cellular processes, such as the regulation of Akt signalling (Gangula and Maddika, 2013; Li et al., 2013), USP12 and USP46 have also non-overlapping functions. On one hand, USP12 regulates the stability of the androgen receptor, the T-cell receptor complex and the Notch receptor, thus modulating signalling through these pathways (Moretti et al., 2012; Burska et al., 2013; McClurg et al., 2014, 2015; Jahan et al., 2016). On the other hand, USP46 regulates the turnover of neuronal AMPA receptors, thus modulating synaptic transmission in the brain (Huo et al., 2015).

It is presently unclear what biological features of USP12 and USP46 may have evolved differentially, correlating with their functional divergence. A crucial aspect in the biology of many enzymes is their targeting to specific subcellular compartments, which may in turn modulate access to their substrates. In this regard, the subcellular localization of human USP12 and USP46 has been a matter of controversy, with different studies describing them as either predominantly cytoplasmic (Sowa et al., 2009; Urbé et al., 2012; Burska et al., 2013; Lehoux et al., 2014; Olazabal-Herrero et al., 2015) or predominantly nuclear proteins (Joo et al., 2011; Jahan et al., 2016). These contrasting observations may reflect a dynamic localization of USP12 and USP46 to different cellular compartments. Supporting this view, both yeast Ubp9 and human USP12 have been shown to undergo nucleocytoplasmic shuttling mediated by the CRM1 nuclear export receptor (Kouranti et al., 2010; Jahan et al., 2016), although the sequence determinants that mediate CRM1-mediated export (i.e. nuclear export sequences or NESs) remain to be confidently identified. Interestingly, the subcellular localization of *S. pombe* Ubp9 was shown to be further regulated by its cofactors Bun107 and Bun62 (Kouranti et al., 2010). These findings raised the possibility that, like their yeast counterparts, human UAF1 and WDR20 might modulate subcellular localization of USP12 and USP46 and, furthermore, that cofactor binding might differentially affect the localization of each DUB.

In the present work, we use siRNA and co-expression approaches, as well as confocal and live microscopy analysis of epitope-tagged proteins to assess the effect of UAF1 and WDR20 on the localization of USP12 and USP46. Our study reveals that USP12 and USP46 have evolved divergently in terms of cofactor binding-regulated subcellular localization. Thus, the steady-state localization of the USP46/UAF1/WDR20 complex was cytoplasmic, while the USP12/UAF1/WDR20 complex localized mainly to the plasma membrane (PM). We further demonstrate that USP12/UAF1/WDR20 shuttles between the PM, cytoplasm and nucleus in a CRM1-dependent manner. From a mechanistic point of view, we show that localization to the PM required direct USP12/WDR20 interaction, as well as the presence of a short amino terminal motif (^{1}MEIL^{4}) in USP12, that is absent in USP46. Furthermore, our data suggest that a previously reported NES in USP12 (Sanyal, 2016) does not act as a relevant nuclear export determinant, and we identify a novel functional NES in WDR20 that mediates CRM1-dependent export of the USP12/UAF1/WDR20 complex. Altogether, our data provide novel insight into how the subcellular localization of these important deubiquitinase complexes is regulated.

2. Material and methods

2.1. Plasmids, cloning procedures and site-directed mutagenesis

Plasmid encoding GFP-USP1 and Xpress-UAF1 were generously provided by Dr. Rene Bernards (Netherlands Cancer Institute, Amsterdam, The Netherlands) and Dr. Jae U. Jung (University of Southern California, Los Angeles, USA), respectively. UAF1-mRFP has been described previously (Olazabal-Herrero et al., 2015). To generate plasmids encoding YFP-USP12, YFP-USP12$^{V279D/F287A}$, YFP-USP12$^{ST/AA}$ and YFP-WDR20, the corresponding cDNA sequences were purchased as gBlocks (IDT), and cloned into pEYFP-C1 (Clontech) using BamHI/HindIII restriction sites. To generate YFP-USP12$^{[+NLSs]}$, USP12 cDNA was cloned into a modified version of pEYFP-C1 containing two copies of the SV40 large T antigen NLS. Myc-WDR20, Myc-USP12, Myc-USP12^{delMEIL} and Myc-USP46 were generated by cloning WDR20, USP12, USP12^{delMEIL} and USP46 cDNAs into pMyc-MCS, a modified version of pEYFP-C1 where the Myc epitope replaces YFP. YFP-USP46 plasmid was obtained by subcloning USP46 cDNA from a previously described plasmid (Olazabal-Herrero et al., 2015) into pEYFP-C1 using BamHI/HindIII restriction sites. To generate YFP-USP12^{delMEIL}, YFP-USP46^{+MEIL} and YFP-WDR20 deletion mutants, the corresponding DNA sequences were amplified by PCR and cloned into pEYFP-C1 using BamHI/HindIII. Finally, Myc-WDR20$^{F262A/W306A}$, Myc-WDR20^{NESm}, YFP-WDR20^{NESm} and YFP-USP12$^{"NES"m}$ mutants were created using the Quick-Change Lightning Site-Directed Mutagenesis Kit (Stratagene).

All the new constructs were subjected to DNA sequencing (STABVIDA). The sequences of the gBlocks and oligonucleotides used in cloning and site-directed mutagenesis are available upon request.

2.2. Cell culture, plasmid and siRNA transfections, and leptomycin B treatment

Human embryonic kidney 293 T cells and HeLa cells were grown in Dulbecco´s modified Eagle´s medium, supplemented with 10% fetal bovine serum, 100 U/ml penicillin and 100 µg/ml streptomycin (all from Invitrogen). Twenty four hours before transfection cells were seeded in 12-well or 10 cm petri dishes. Plasmid transfections were carried out with X-tremeGENE 9 transfection reagent (Roche Diagnostics) following manufacturer's protocol. For knockdown experiments, cells were transfected with a pool of three siRNAs included in the TriFECTa RNAi Kits (IDT) targeting WDR20 (hs.Ri.WDR20.13) or UAF1 (hs.Ri.WDR48.13). Scramble silencer select siRNA #1 (Ambion, Life Technologies) was used as a negative control. siRNA transfections were carried out using Lipofectamine RNAiMAX (Invitrogen) following manufacturer's protocol.

Leptomycin B (LMB; Apollo Scientific) was added to the culture medium to a final concentration of 6 ng/ml for the indicated period of time.

2.3. Immunofluorescence, microscopy and image analysis

Cells were fixed with 3.7% formaldehyde in PBS for 30 min, permeabilized with 0.2% Triton X-100 in PBS for 10 min, blocked for 1 h in blocking solution (3% BSA in PBS) and incubated with primary antibodies diluted in blocking solution for 1 h at room temperature. Anti-Myc (Cell Signaling Technology; 1:300) and anti-pSer473-Akt (Cell Signaling Technology; 1:100) were used as primary antibodies. Cells were then washed and incubated with secondary antibodies (Alexa Fluor 594-conjugated anti-mouse/rabbit IgG and Alexa Fluor 633-conjugated anti-mouse IgG; Invitrogen; 1:400) for 1 h at room temperature. Coverslips were washed and mounted onto microscope slides using

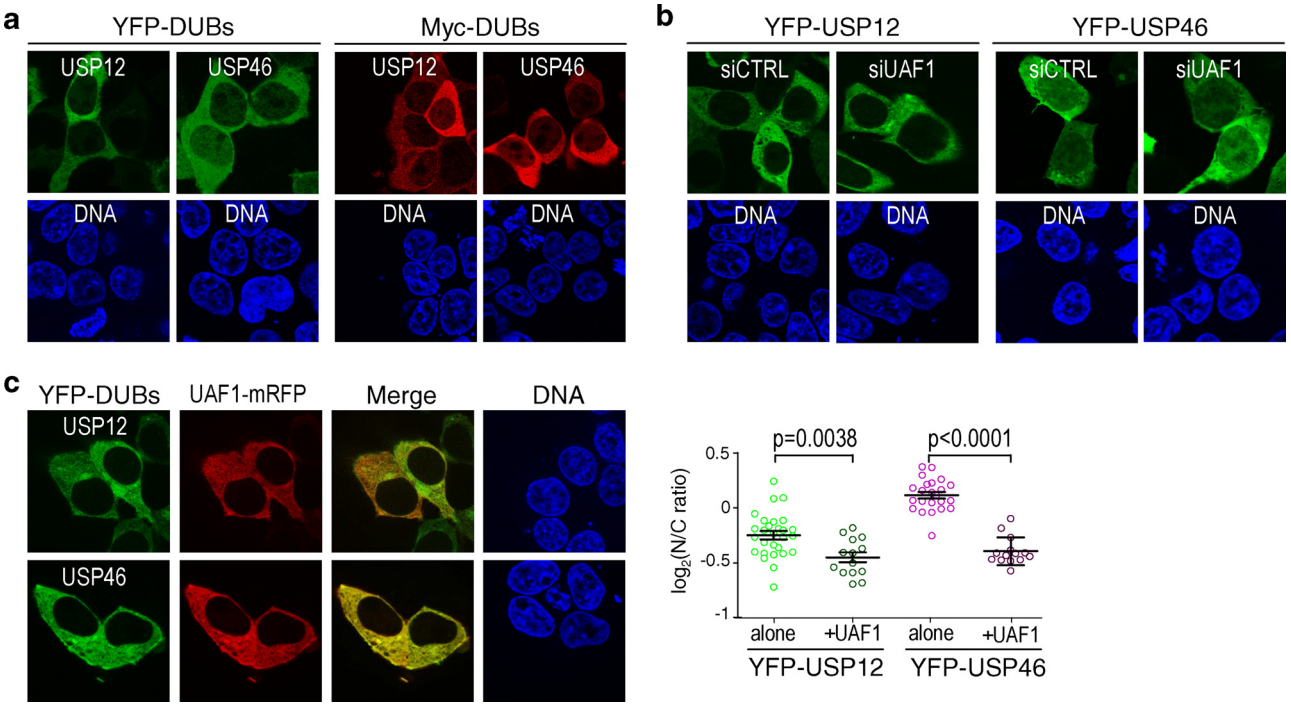

Fig. 1. Co-expression with UAF1 increases the cytoplasmic localization of USP12 and USP46.
a Confocal microscopy images show representative examples of 293 T cells expressing YFP- or Myc-tagged USP12 and USP46. DAPI was used to visualize the nuclei (DNA panels). **b** Representative examples of YFP-USP12 and YFP-USP46 localization in 293 T cells transfected with a scramble siRNA control (siCTRL) or with a pool of three siRNAs targeting UAF1 (siUAF1). **c** Confocal images of 293 T cells co-expressing YFP-USP12 or YFP-USP46 with UAF1-mRFP. Using image analyses, the intensity of the YFP signal in the nucleus and cytoplasm was quantified to calculate the nuclear to cytoplasmic (N/C) ratio. Each circle in the graph represents a single cell, and the mean (+/- SD) is also indicated. The data correspond to a single experiment, where 15–30 individual cells per condition were analysed. Comparable results were obtained in several independent experiments. The p values (Mann-Whitney U test) are indicated.

Vectashield mounting medium containing DAPI (Vector Laboratories). Single-slice images were acquired using a Zeiss ApoTome.2 microscope.

For live cell imaging, cells were grown in 35 mm IbiTreat μ-dish slides (Ibidi), and examined using a LEICA LCS SP2 AOBS microscope fitted with a temperature-controlled chamber.

Image analysis was carried out using Fiji (Schindelin et al., 2012). The "Linescan" tool and the "Coloc2" plug-in were used to assess co-localization of proteins. An ad-hoc script was developed to automatically quantify fluorescence intensity in nuclear and cytoplasmic regions using the MorphoLibJ library (Legland et al., 2016). Data were analysed using the Mann-Whitney U test and $p < 0.005$ were considered statistically significant.

2.4. Fluorescence recovery after photobleaching (FRAP) analysis

HeLa cells were grown in 35 mm ibiTreat μ-dish slides (Ibidi). Twenty four hours after transfection, FRAP analysis was carried out using a LEICA LCS SP2 AOBS microscope. The excitation (acquisition) laser was set at 10% power and the region of interest was bleached by 100% laser power. Five pre-bleach and thirty five post-bleach images were collected for each cell, with a 1.6 s time interval. Images were processed using Fiji (Schindelin et al., 2012), and data were analysed using GraphPad Prism. Halftime of recovery ($t_{1/2}$) and mobile fraction (F_m) were calculated as described in (http://www.embl.de/eamnet/frap/html/overview.html).

2.5. Sequence alignment and prediction of candidate nuclear export sequences (NESs)

Multiple sequence alignment was carried out with Clustal Omega (https://www.ebi.ac.uk/Tools/msa/clustalo/).

To identify candidate NESs, the amino acid sequence of WDR20 was analysed using the NES prediction tool WREGEX (http://ehubio.ehu.eus/wregex) (Prieto et al., 2014).

2.6. Rev(1.4)-GFP based nuclear export assay

In order to test the activity of candidate NESs, the pRev(1.4)–GFP-based nuclear export assay was carried out as reported previously (Henderson and Eleftheriou, 2000). Rev(1.4)–GFP is a chimaeric protein resulting from the fusion of an export-deficient (NES mutated) version of the HIV Rev protein to GFP. The Rev(1.4) protein bears an intact nuclear localization signal (NLS), and Rev(1.4)–GFP localizes to nucleoli. Candidate NESs are cloned between the Rev(1.4) and the GFP moieties, and active nuclear export signals are identified based on their ability to induce Rev(1.4)–GFP relocation to the cytoplasm. ActD, which disrupts nucleoli and blocks nuclear import mediated by Rev (1.4) NLS, is added to reveal the activity of weaker NESs. Double-stranded DNA fragments encoding USP12 sequence ^{75}RKKESLLTCLADLFHSIAT^{93} and WDR20 sequence ^{450}MDGAIASGVSKFATLSLHD^{468} were cloned into the Rev(1.4)-GFP reporter vector (a gift from Dr. Beric Henderson, University of Sydney, Australia) using BamHI/PinAI restriction sites. These plasmids, termed Rev(1.4)-[NES^{USP12}]-GFP and Rev(1.4)-[cNES^{WDR20}]-GFP, respectively, were transfected into HeLa cells. The empty Rev(1.4)-GFP reporter was included as negative control. Each plasmid was transfected in two wells. At 24 h post-transfection, one of the wells per sample was treated with 10 μg/ml cycloheximide (CHX; Sigma) and the other was treated with10 μg/ml CHX (Sigma) plus 5 μg/ml actinomycin D (ActD; Sigma). CHX is added to arrest protein translation and thus ensure that cytoplasmic GFP signal arises from nuclear export and not from newly synthesized proteins. Three hours after treatment, cells were fixed and mounted for microscopy analysis. Using a Zeiss Axioskop fluorescence microscope, the subcellular localization of the GFP-tagged proteins was determined in at

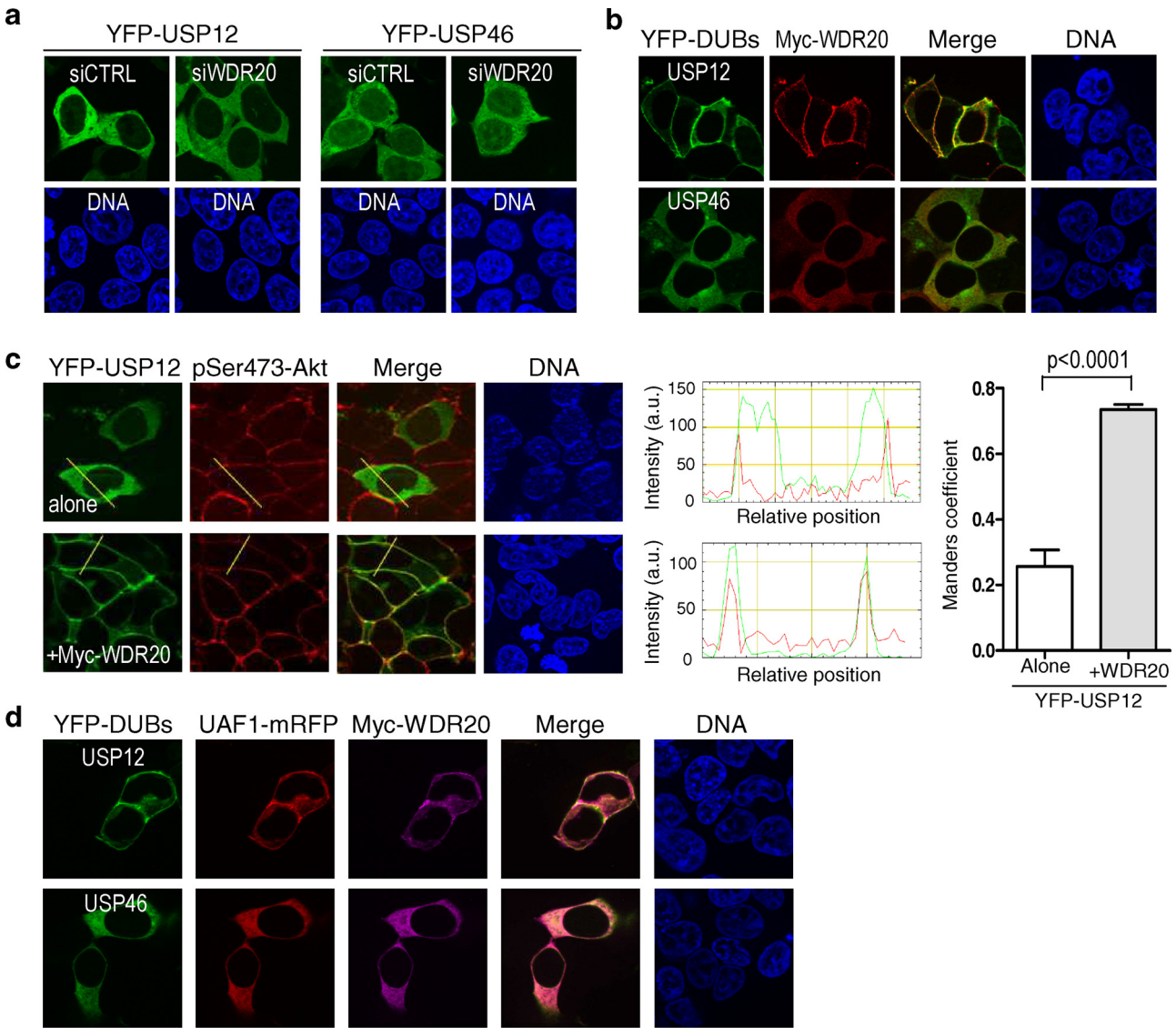

Fig. 2. Co-expression with WDR20 induces translocation of USP12, but not USP46 to the plasma membrane.
a Confocal microscopy images show representative examples of YFP-USP12 and YFP-USP46 localization in 293 T cells transfected with a scramble siRNA control (siCTRL) or with a pool of three siRNAs targeting WDR20 (siWDR20). **b** Representative examples of 293 T cells co-expressing YFP-USP12 or YFP-USP46 with Myc-WDR20. YFP-USP12 co-localizes with Myc-WDR20 at the cell periphery, whereas YFP-USP46 and Myc-WDR20 diffusely co-localize throughout the cytoplasm. **c** *Left.* Confocal images of 293 T cells transfected with YFP-USP12 alone or co-transfected with YFP-USP12 and Myc-WDR20. Cells were stained with an antibody to detect endogenous pSer473-Akt, a protein that transiently associates with the plasma membrane (PM). *Middle.* The Fiji "Linescan" tool was used to determine the intensity of the fluorescent signal along the yellow lines indicated in the images. The overlap between the green (YFP-USP12) and the red (pSer473-Akt) increases when the DUB is co-expressed with Myc-WDR20. *Right.* Graph shows the Manders correlation coefficient indicating the extent of YFP-USP12/pSer473-Akt co-localization in multiple (n > 100) cells transfected with either YFP-USP12 alone or co-transfected with YFP-USP12 and Myc-WDR20. The analysis was carried out using the "Coloc2″ plugin from Fiji. Data represent the mean, and error bars indicate standard deviation (+/- SD). The p value (Student´s t-test) is indicated. **d** Confocal images of 293 T cells co-expressing YFP-USP12 or YFP-USP46 with UAF1-mRFP and Myc-WDR20. YFP-USP12 and its cofactors co-localized mostly at the cell periphery, suggesting recruitment of the complex to the PM. In contrast, YFP-USP46 and its cofactors co-localized diffusely in the cytoplasm.

least 200 cells per sample. Based on the proportion of cells showing nuclear, nuclear and cytoplasmic or cytoplasmic GFP signal, the level of export activity of the candidate NES was rated between 0 (non-functional) and 9+ using the assay scoring system (Henderson and Eleftheriou, 2000).

2.7. Co-immunoprecipitation analysis

Cells were lysed using IP Lysis buffer (Pierce), and lysates were subjected to anti-GFP immunoprecipitation using the GFP-Trap_MA reagent (Chromotek), following manufacturer´s directions. Immunoprecipitated proteins were analysed by immunoblot. To this end, protein samples were loaded into 10% SDS-PAGE gel, resolved by electrophoresis, and transferred to a nitrocellulose membrane. Membranes were blocked with 5% non-fat dry milk diluted in TTBS for 1 h and incubated with the primary antibodies: anti-Myc (Cell Signaling Technology, 1:2000), anti-GFP (Chromotek, 1:1000) or anti-Xpress (Invitrogen, 1:5000). Subsequently, membranes were incubated with the corresponding horseradish peroxidase-conjugated secondary antibody (Santa-Cruz, 1:3000), washed and developed using ECL (Thermo Scientific).

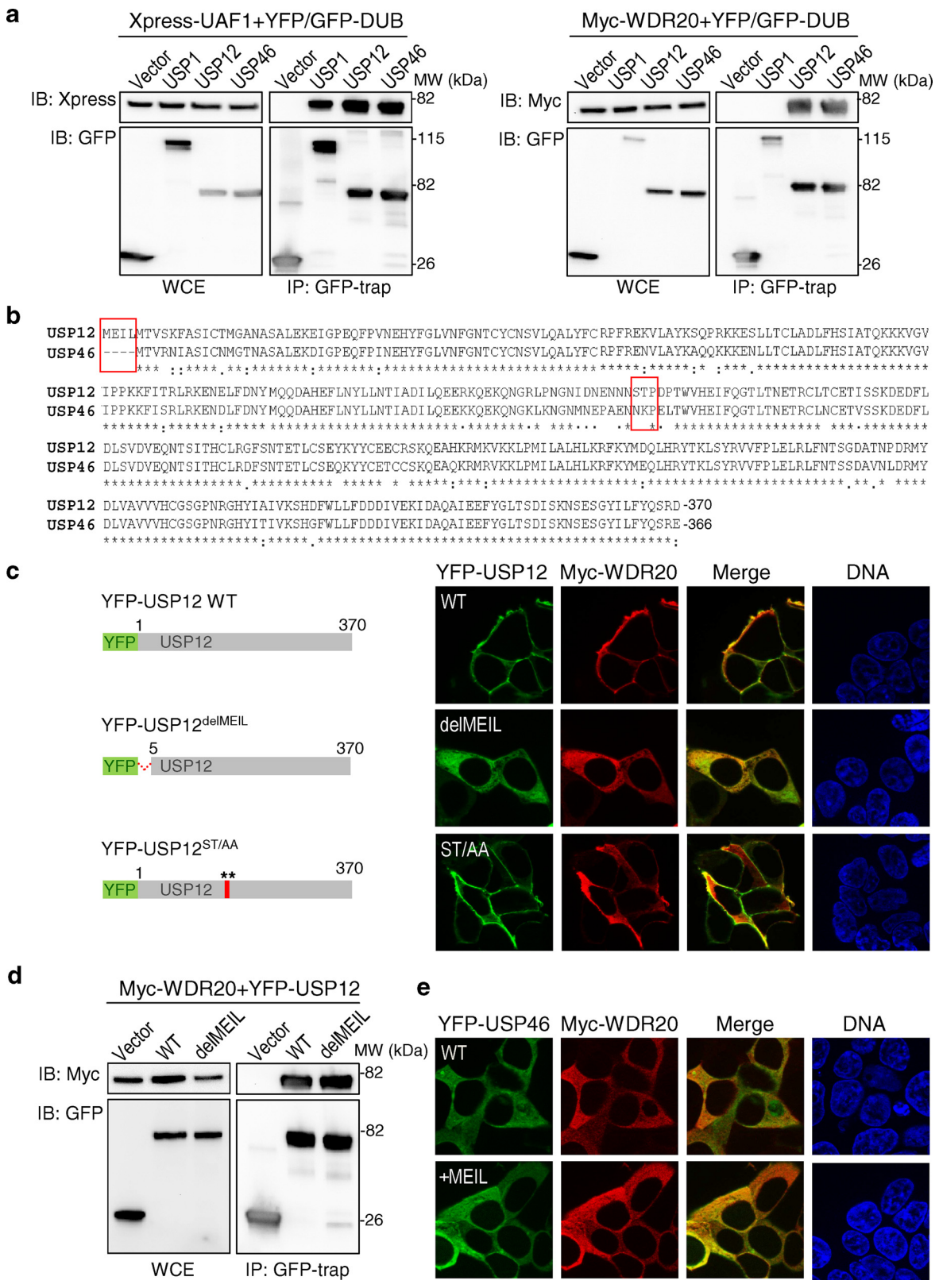

(caption on next page)

Fig. 3. A short motif in USP12, absent in USP46, contributes to plasma membrane localization of USP12/WDR20.
a. Co-immunoprecipitation (Co-IP) analyses of 293 T cells co-transfected with YFP-vector (negative control), GFP-USP1 (which is known to interact with UAF1 but not with WDR20), YFP-USP12 or YFP-USP46 and either Xpress-UAF1 (*left*) or Myc-WDR20 (*right*). Whole cell extracts (WCE) and proteins immunoprecipitated using the GFP-trap reagent were analyzed by immunoblot (IB) using anti-GFP, anti-Xpress or anti-Myc antibodies, as indicated. As expected, Xpress-UAF1 was efficiently co-immunoprecipitated by the three DUBs (*left panels*). Importantly, Myc-WDR20 was co-immunoprecipitated to a similar extent by YFP-USP12 and YFP-USP46, but not by GFP-USP1 (*right panels*). These results strongly suggest that the different effect of WDR20 on the localization of USP12 and USP46 is not due to differential binding of WDR20 to each DUB in our experimental setting. **b** Alignment of USP12 and USP46 amino acid sequences using Clustal Omega. Red squares highlight a short N-terminal motif (^{1}MEIL^{4}) and a potential minimal MAPK phosphorylation motif (^{165}STP^{167}) that are present in USP12 but not in USP46. **c** *Left.* Schematic representation of wild type YFP-USP12, and the mutants lacking the ^{1}MEIL^{4} motif (YFP-USP12^{delMEIL}) or the potential phosphorylation site (YFP-USP12$^{ST/AA}$). *Right.* Confocal images of 293 T cells co-expressing either wild type YFP-USP12, YFP-USP12^{delMEIL} or YFP-USP12$^{ST/AA}$ and Myc-WDR20. YFP-USP12^{delMEIL} mutant is not translocated to the PM when co-expressed with Myc-WDR20. **d** Blots show the results of co-immunoprecipitation (co-IP) analyses in 293 T cells showing that deletion of the ^{1}MEIL^{4} motif does not disrupt USP12/WDR20 interaction. Whole cell extracts (WCE) and proteins immunoprecipitated using the GFP-trap reagent were analyzed by immunoblot (IB) using the indicated antibodies. **e** Confocal images of 293 T cells co-expressing Myc-WDR20 with either wild type YFP-USP46 or YFP-USP46^{+MEIL}. Addition of the MEIL motif to the amino-terminal end of USP46 is not sufficient to confer WDR20-induced PM recruitment.

3. Results

3.1. Co-expression with UAF1 increases cytoplasmic localization of USP12 and USP46

We began our analysis by comparing the subcellular localization of human USP12 and USP46. The amino acid sequence of USP12 and USP46 is nearly 90% identical. To prevent confounding effects due to potential cross-reactivity of antibodies against these DUBs (Joo et al., 2011), we generated tagged versions of USP12 and USP46 fused to YFP or Myc epitopes. The subcellular localization of these proteins was assessed in transfected 293 T cells by confocal microscopy. Both DUBs, fused to either YFP or Myc (Fig. 1a), were predominantly located in the cytoplasm. A faint fluorescent signal was noticeable in the nucleus of some cells expressing USP12 and, more prominently, USP46. We also generated epitope-tagged versions of the two cofactors (UAF1-mRFP and Myc-WDR20), which were located to the cytoplasm (Additional File 1a).

In order to asses a potential effect of UAF1 on the localization of YFP-USP12 and YFP-USP46, cellular levels of UAF1 were either reduced using small interfering RNA (siRNA)-mediated knockdown or increased using UAF1-mRFP transfection. UAF1 knockdown was carried out with a pool of three siRNA oligonucleotides that consistently reduces UAF1 expression (Additional File 1b,c). As shown in Fig. 1b, UAF1 knockdown had no obvious effect on the localization of YFP-USP12 or YFP-USP46. On the other hand, YFP-USP12 and YFP-USP46 co-localized with UAF1-mRFP throughout the cytoplasm in co-transfection experiments (Fig. 1c) and, as shown by image analysis, co-expression with UAF1 markedly reduced the nuclear-to-cytoplasmic (N/C) ratio of both DUBs.

3.2. Co-expression with WDR20 induces translocation of USP12, but not USP46, to the plasma membrane

We used a similar knockdown/overexpression approach to asses a potential effect of WDR20 on the localization of YFP-USP12 and YFP-USP46. Similar to UAF1 knockdown, WDR20 siRNA had no obvious effect on the localization of YFP-USP12 or YFP-USP46 (Fig. 2a). However, we found that WDR20 co-expression had a strikingly different effect on the localization of each DUB. Whereas YFP-USP46 and Myc-WDR20 co-localized diffusely throughout the cytoplasm, YFP-USP12 and Myc-WDR20 co-localized at the cell periphery (Fig. 2b). Although less pronounced, a similar localization to the cell periphery was observed with Myc-tagged USP12, when co-expressed with YFP-WDR20 (Additional File 2a).

The localization of co-expressed USP12 and WDR20 suggested recruitment to the plasma membrane (PM). To further confirm this possibility, we carried out immunostaining with an antibody that recognizes endogenous Akt1 phosphorylated at Ser473 (hereafter termed pSer473-Akt). This phosphorylation event occurs at the PM, where pSer473-Akt remains transiently located (Manning and Toker, 2017). As expected, the co-localization of YFP-USP12 with PM-located pSer473-Akt significantly increased upon co-transfection with Myc-WDR20 (Fig. 2c).

Finally, we used triple co-transfection experiments to evaluate the localization of the ternary USP12/UAF1/WDR20 and USP46/UAF1/WDR20 complexes. Co-expressed YFP-USP12/UAF1-mRFP/Myc-WDR20 co-localized to the PM (Fig. 2d), whereas YFP-USP46/UAF1-mRFP/Myc-WDR20 diffusely co-localized in the cytoplasm.

Altogether, these results suggest that WDR20 binding promotes translocation of USP12/WDR20 to the plasma membrane, facilitating the recruitment of the USP12/UAF1/WDR20 complex to this subcellular compartment. In contrast, the steady-state localization of the USP46/UAF1/WDR20 complex is predominantly cytoplasmic.

Our finding that WDR20 differently modulates the localization of USP12 and USP46 led us to investigate the factors that may underlie this difference, as well as to further characterize the mechanisms that modulate the subcellular localization of the USP12 deubiquitinase complex.

3.3. A short amino acid motif in USP12, not present in USP46, contributes to plasma membrane localization of the USP12/WDR20 complex

We first used co-immunoprecipitation (co-IP) to rule out the possibility that the different effect of WDR20 on the localization of USP12 and USP46 was related to a different ability of the cofactor to bind these DUBs in our experimental system (Fig. 3a). Next, we considered the possibility that the different localization of USP12 and USP46 when co-expressed with WDR20 might be related to small differences in their amino acid sequence. We noticed that USP12 bears a four amino-acid motif at its extreme N-terminal end (^{1}MEIL^{4}) and a potential minimal MAPK phosphorylation motif (^{165}STP^{167}) (Bardwell, 2006), which are absent in USP46 (Fig. 3b). We generated USP12 mutant versions lacking these motifs (USP12^{delMEIL} and USP12$^{ST/AA}$). As shown in Fig. 3c, the ability of YFP-USP12^{delMEIL} mutant to relocate to the PM when co-expressed with Myc-WDR20 was virtually abrogated. A similar result was obtained using Myc-tagged USP12 and YFP-tagged WDR20 (Additional File 2b). In contrast, the YFP-USP12$^{ST/AA}$ mutant still co-localized with Myc-WDR20 to the PM. Importantly, co-IP analysis (Fig. 3d) showed that YFP-USP12^{delMEIL} interacts with Myc-WDR20 as efficiently as wild type YFP-USP12. We next added the MEIL motif to the N-terminal end of USP46. However, YFP-USP46^{+MEIL} remained in the cytoplasm when co-expressed with Myc-WDR20 (Fig. 3e).

Together, these results indicate that the amino-terminal ^{1}MEIL^{4} motif is necessary for the efficient recruitment of USP12/WDR20 to the PM, but is not sufficient to confer PM localization to a USP46/WDR20 complex.

3.4. Plasma membrane recruitment of YFP-USP12 requires direct binding to WDR20

The co-expression experiments described above are carried out in a

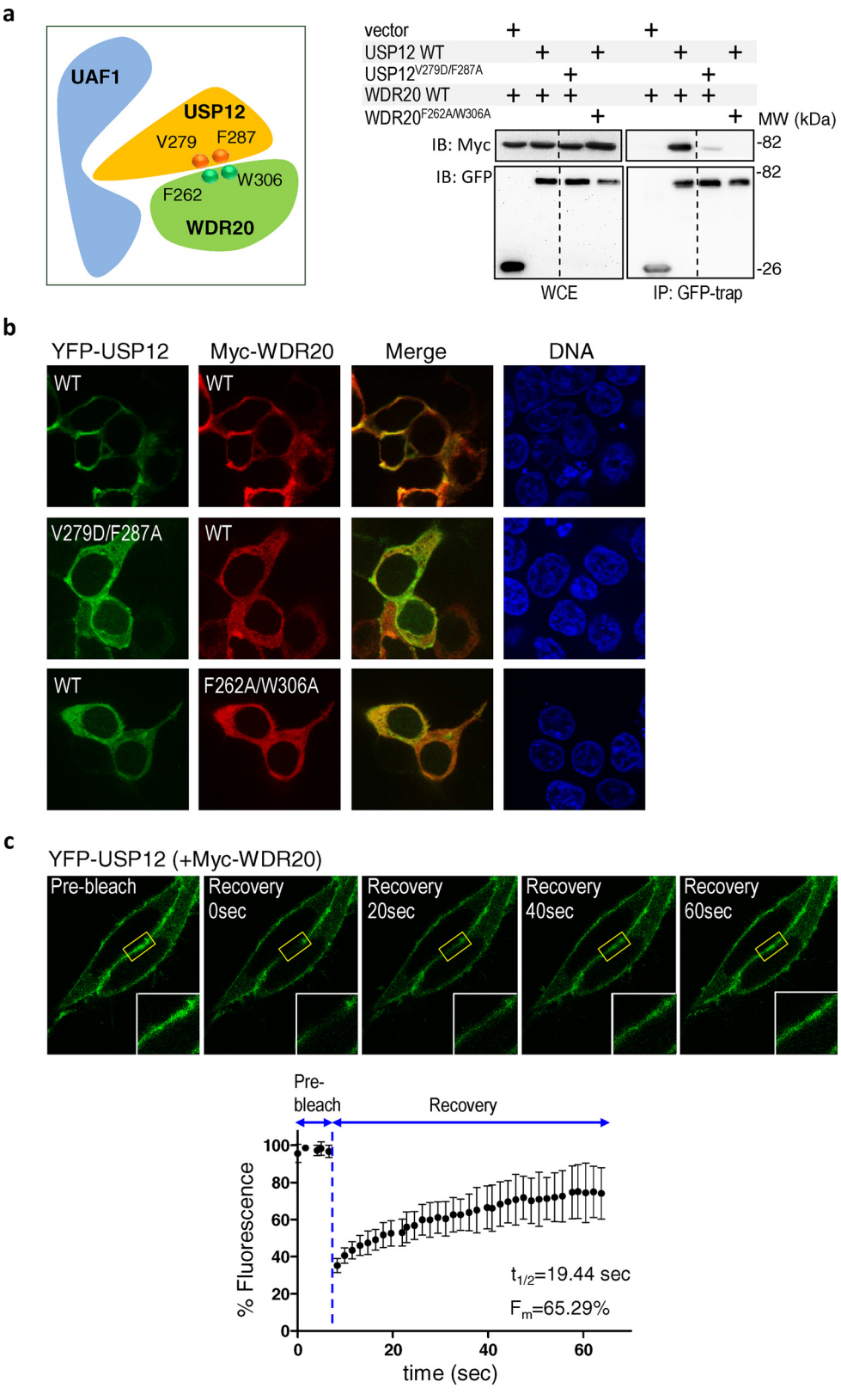

Fig. 4. Plasma membrane recruitment of USP12 requires binding to WDR20 and is highly dynamic.

a *Left.* Schematic representation of the USP12/UAF1/WDR20 complex, based on the reported three-dimensional structure (Li et al., 2016), showing the amino acids whose mutation has been shown to disrupt USP12/WDR20 interaction. *Rigth.* Blots showing the results of co-IP analysis of 293 T cells co-transfected with the indicated plasmids. The ability of YFP-USP12$^{V279D/F287A}$ to bind Myc-WDR20 is severely reduced, and Myc-WDR20$^{F262A/W306A}$ is unable to bind YFP-USP12. **b** Confocal images of 293 T cells showing that mutations that disrupt USP12/WDR20 binding abolish the translocation of co-expressed YFP-USP12 and Myc-WDR20 to the PM. **c** Representative example of fluorescence recovery after photobleaching (FRAP) analysis in live HeLa cells co-transfected with YFP-USP12 and Myc-WDR20. YFP-USP12 signal was bleached in a region of the PM (yellow rectangle), and the fluorescence recovery was followed during 65 s. Insets show a magnified image of the bleached region. Below, the recovery curve represents the average of 5 individual cells. Error bars indicate the SD. Halftime of recovery ($t_{1/2}$) and mobile fraction (F_m) values are indicated inside the graph.

complex cellular setting. It might be argued that co-expression of WDR20 might indirectly promote PM recruitment without requiring the formation of a USP12/WDR20 complex. To address this possibility, we made use of the information provided by a recent study (Li et al., 2016), where the three-dimensional structure of a ternary USP12/UAF1/WDR20 complex was reported, identifying critical residues in USP12 (V279 and F287) and WDR20 (F262 and W306) (Fig. 4a) whose mutation disrupts USP12/WDR20 interaction (Li et al., 2016). We generated YFP-USP12$^{V279D/F287A}$ and Myc-WDR20$^{F262A/W306A}$ mutants and confirmed that these mutations largely or completely abrogate WDR20 binding to USP12 in 293 T cells (Fig. 4a). As shown in Fig. 4b, YFP-USP12$^{V279D/F287A}$ did not relocate to the PM when co-expressed with

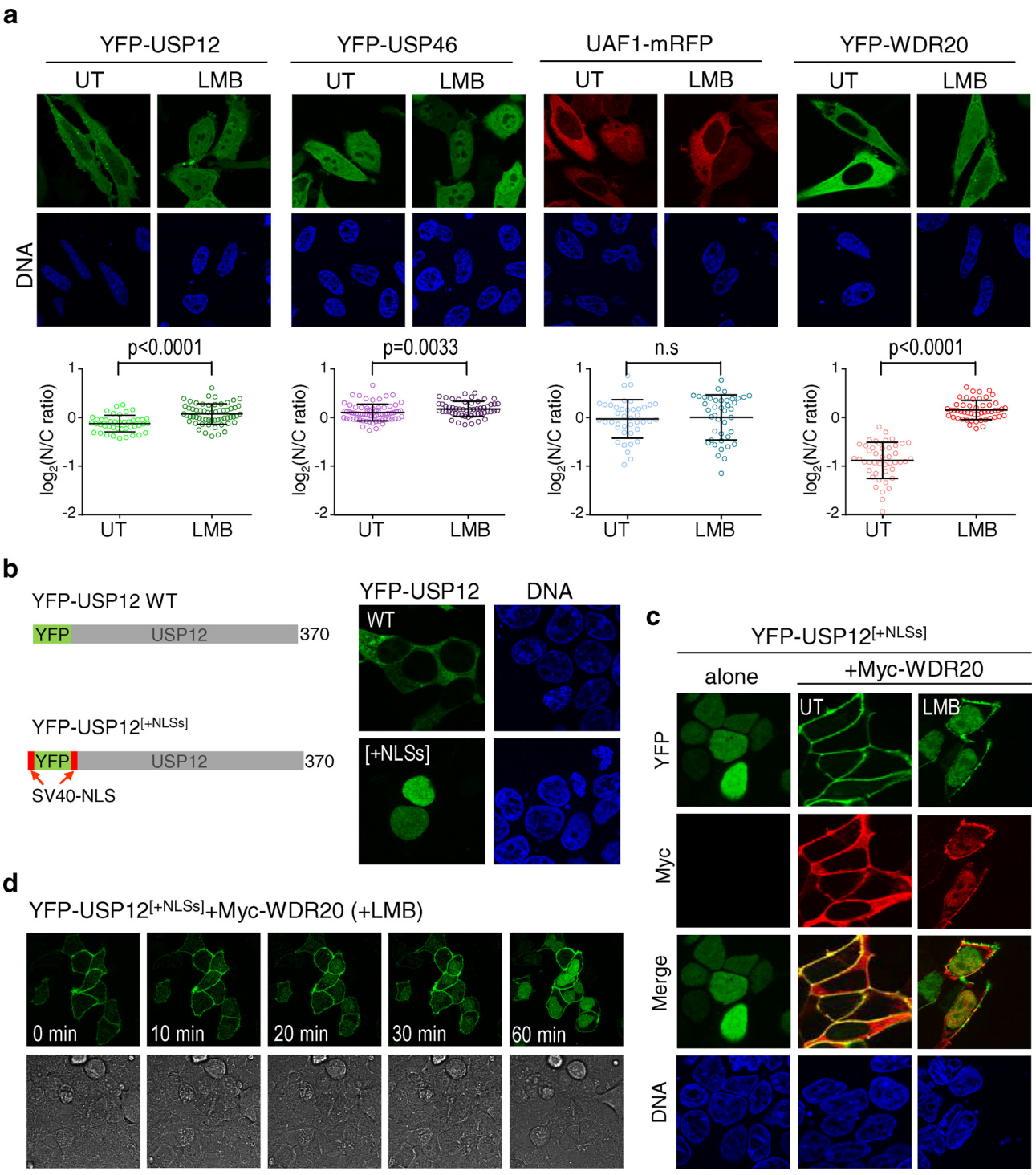

Fig. 5. CRM1-mediated nuclear export facilitates shuttling of USP12/WDR20 between the plasma membrane, cytoplasm and nucleus.
a Representative examples of the nucleocytoplasmic localization of YFP-USP12, YFP-USP46, UAF1-mRFP and YFP-WDR20 in HeLa cells untreated (UT) or treated with the CRM1 inhibitor leptomycin B (LMB) (6 ng/ml for 3 h). The N/C ratio of each protein in untreated or LMB-treated cells was determined using image analysis and is shown in the graphs below. Each circle in the graph represents a single cell, and the mean (+/- SD) is also indicated. The data correspond to a single experiment where at least 40 transfected cells per condition were analysed. Comparable results were obtained in at least two independent experiments. p values (Mann-Whitney U test) are indicated (n.s: non-significant). **b** *Left.* Schematic representation of wild type YFP-USP12 and YFP-USP12$^{[+NLSs]}$, a variant tagged with two copies of the SV40 large T antigen nuclear localization signal (SV40-NLS; in red). *Right.* Confocal images of 293 T cells showing nuclear accumulation of YFP-USP12$^{[+NLSs]}$. **c** Confocal images of 293 T cells expressing YFP-USP12$^{[+NLSs]}$ alone or co-expressing YFP-USP12$^{[+NLSs]}$ and Myc-WDR20. YFP-USP12$^{[+NLSs]}$ and Myc-WDR20 co-localize to the PM in untreated cells (UT), but partially relocalize to the nucleus after LMB treatment (6 ng/ml LMB for 3 h). **d** Confocal images of a time-lapse experiment in live 293 T cells co-expressing YFP-USP12$^{[+NLSs]}$ and Myc-WDR20. After treating the cells with LMB (6 ng/ml), the localization of YFP-USP12$^{[+NLSs]}$ was examined and recorded every 2 min for 1 h. Brightfield images at each time point are shown below. YFP-USP12$^{[+NLSs]}$ was detectable in the nucleus 10 min after LMB addition.

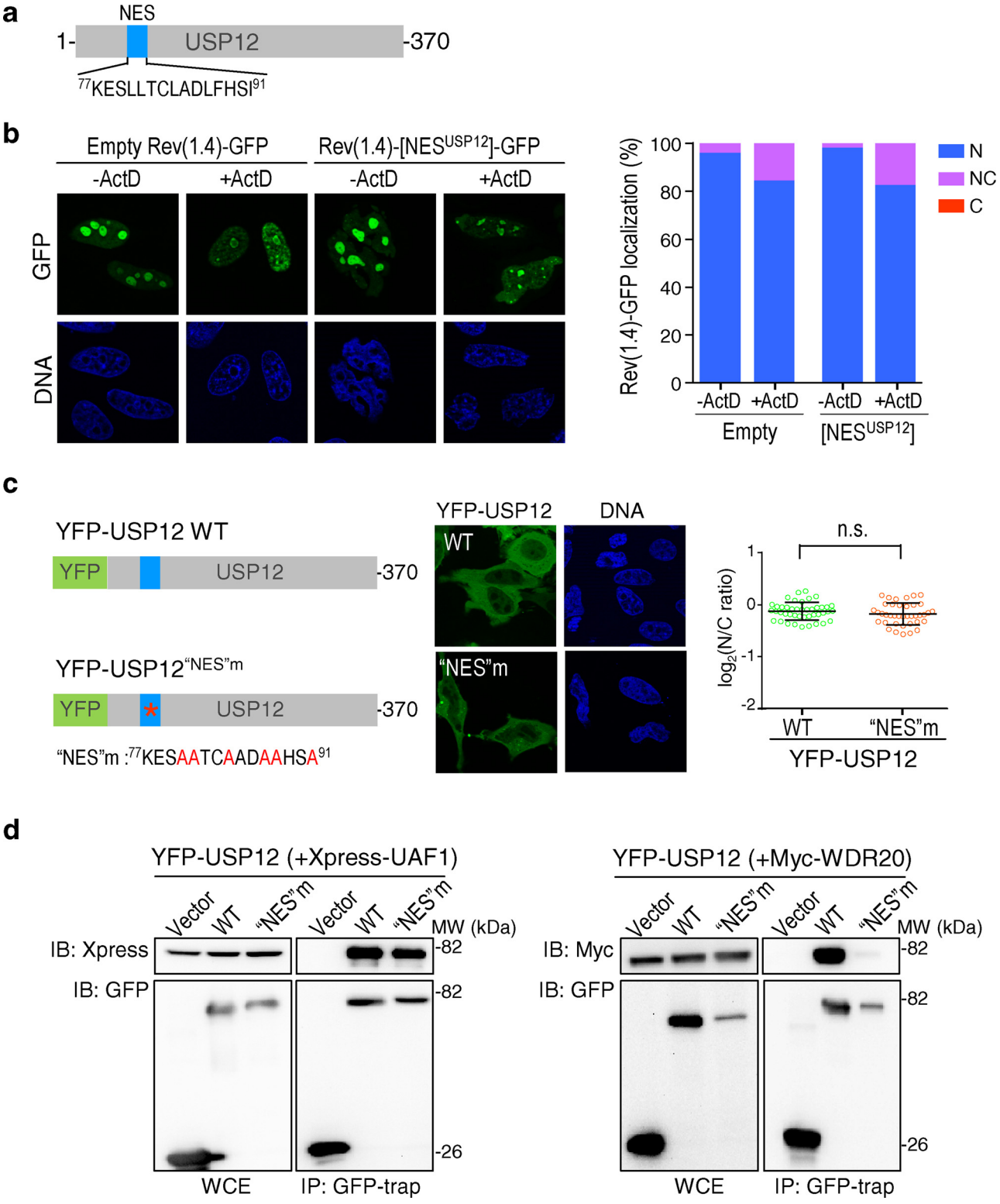

(caption on next page)

wild type Myc-WDR20, and conversely, co-expression with Myc-WDR20$^{F262A/W306A}$ did not result in PM localization of wild type YFP-USP12.

Although it cannot be formally ruled out that the introduced mutations may affect folding of the proteins and thus indirectly affect localization, this is unlikely in our view, considering that only two point mutations (and not large deletions or multiple aminoacid changes) are introduced in each protein. Thus, we believe that these findings indicate that direct binding to WDR20 is required for PM localization of USP12.

Fig. 6. A previously described NES in USP12 is not a direct nuclear export determinant.
a Schematic representation of USP12 showing the position and amino-acid sequence of a previously described NES motif (Jahan et al., 2016; Sanyal, 2016). **b** Results of a nuclear export assay to test the activity of this motif. The assay is based on the ability of functional NESs to promote export of the nuclear reporter protein Rev (1.4)-GFP to the cytoplasm (Henderson and Eleftheriou, 2000). As described in detail in the Methods section, actinomycin D (ActD) allows detection of weak NESs. *Left*. Confocal images showing representative examples of HeLa cells transfected with the empty Rev(1.4)-GFP reporter plasmid or with the plasmid Rev(1.4)-[NES^{USP12}]-GFP, containing the reported USP12 NES. *Right.* Graph showing the percentage of cells with mostly nuclear (N), nuclear and cytoplasmic (NC) or mostly cytoplasmic (C) localization of the reporter. At least 200 transfected cells were scored per condition. Even in the presence of ActD, the described USP12 NES motif was unable to promote nuclear export of Rev(1.4)-GFP. **c** *Left*. Schematic representation of wild type YFP-USP12 and a previously used "NES" mutant (YFP-$USP12^{"NES"m}$) bearing six amino-acid substitutions indicated in red (Jahan et al., 2016; Sanyal, 2016). *Center*. Confocal images of HeLa cells expressing YFP-USP12 and YFP-$USP12^{"NES"m}$. *Right*. Graph showing the N/C ratio of both proteins determined using image analysis of at least 30 transfected cells per sample. Each circle in the graph represents a single cell, and the mean (+/- SD) is shown. n.s: non-significant (Mann-Whitney U test). **d**. Results of co-IP analyses in 293 T cells co-transfected with YFP vector, wild type YFP-USP12 or YFP-$USP12^{"NES"m}$ and either Xpress-UAF1 (left) or Myc-WDR20 (right). The six mutations introduced into the "NES" motif of USP12 do not interfere with UAF1 interaction, but completely abrogate WDR20 binding.

3.5. WDR20-induced localization of YFP-USP12 to the plasma membrane is highly dynamic

To further characterize the PM localization of USP12, we carried out fluorescence recovery after photobleaching (FRAP) experiments. As in 293 T cells, YFP-USP12 also localized to the PM in live HeLa cells when co-expressed with Myc-WDR20 (Fig. 4c). The YFP-USP12 fluorescent signal was rapidly recovered in an area of the PM where it had been bleached. The calculated halftime of recovery ($t_{1/2}$) and mobile fraction (F_m) values were 19.44 s and 65.29%, respectively, indicating that the PM localization of YFP-USP12 is highly dynamic.

3.6. CRM1-mediated nuclear export facilitates shuttling of USP12/WDR20 between the plasma membrane, cytoplasm and nucleus

Together with the recent finding that USP12 can be exported from the nucleus to the cytoplasm by CRM1 (Jahan et al., 2016), our results raised the possibility that the USP12/WDR20 complex may undergo dynamic shuttling between the PM, cytoplasm and nucleus.

We tested the effect of the specific CRM1 inhibitor leptomycin B (LMB) on the nucleocytoplasmic distribution of epitope-tagged USP12, USP46, UAF1 and WDR20 in HeLa cells. As shown in Fig. 5a, a three hour LMB treatment did not alter the distribution of UAF1-mRFP. A statistically significant, but very limited, increase in the N/C ratio of YFP-USP46 was noted. The clearest and most statistically significant effect of LMB was on YFP-USP12 and, particularly, on YFP-WDR20, indicating that both proteins are actively exported from the nucleus by the CRM1-mediated nuclear export pathway.

Of note, YFP-USP12 and YFP-WDR20 were evenly distributed between nucleus and cytoplasm in LMB-treated cells, but they did not accumulate to a high level inside the nucleus. This observation suggests that the nuclear entry of these proteins is not a highly efficient process, which could be due to cytoplasmic retention or to the lack of strong nuclear localization signals (NLSs). To gauge these possibilities, we generated a version of YFP-USP12 bearing two copies of the strong SV40 large T antigen NLS (YFP-$USP12^{[+NLSs]}$) (Fig. 5b). YFP-$USP12^{[+NLSs]}$ readily accumulated into the nucleus, suggesting that YFP-USP12 inefficient import into the nucleus is most likely due to the lack of strong NLSs. Of note, a faint fluorescent signal at the PM was also noticeable in some cells expressing YFP-$USP12^{[+NLSs]}$ alone, probably due to the presence of endogenous WDR20.

The efficient nuclear import of YFP-$USP12^{[+NLSs]}$ provided a convenient experimental tool to test our hypothesis that USP12/WDR20 may shuttle between the PM, cytoplasm and nucleus. Despite the presence of the strong SV40 NLSs, YFP-$USP12^{[+NLSs]}$ localized to the PM when co-expressed with Myc-WDR20 (Fig. 5c) in 293 T cells. A similar result was obtained using Myc-tagged $USP12^{[+NLSs]}$ and YFP-tagged WDR20 (Additional File 2c). Importantly, YFP-$USP12^{[+NLSs]}$ and Myc-WDR20 partially relocated to the nucleus when CRM1-mediated export was inhibited by LMB treatment. In fact, live microscopy experiments revealed that YFP-$USP12^{[+NLSs]}$ was detectable in the nucleus only a few minutes after LMB addition (Fig. 5d).

These observations indicate that the USP12/WDR20 complex is able to dynamically shuttle between PM, cytoplasm and nucleus.

3.7. A previously described NES in USP12 is not a direct nuclear export determinant

The USP12 motif ^{77}KESLLTCLADLFHSI^{91} (Fig. 6a) has been recently proposed to be a CRM1-dependent NES, although its putative export function has not been characterized (Jahan et al., 2016; Sanyal, 2016). We tested a USP12 fragment containing this motif and flanking residues (^{75}RKKESLLTCLADLFHSIAT^{93}) using a nuclear export assay (Henderson and Eleftheriou, 2000) based on the ability of functional NESs to confer cytoplasmic localization to an otherwise nuclear reporter termed Rev (1.4)-GFP. As shown in Fig. 6b, the proposed USP12 NES was unable to increase the cytoplasmic localization of the Rev(1.4)-GFP reporter, even in the presence of actinomycin D (ActD), a drug used in this assay to identify very weak NESs (Henderson and Eleftheriou, 2000). The USP12 motif ^{77}KESLLTCLADLFHSI^{91} was therefore classified as a non-functional NES-like motif, and hereafter we refer to this motif as USP12 "NES".

Mutation of six residues within this "NES" has been previously reported to interfere with USP12 nuclear export in Jurkat cells (Jahan et al., 2016). We introduced these mutations into YFP-USP12 to generate YFP-$USP12^{"NES"m}$. The nucleocytoplasmic distribution of YFP-$USP12^{"NES"m}$ was identical to that of YFP-USP12 in HeLa cells (Fig. 6c), further supporting our view that the motif ^{77}KESLLTCLADLFHSI^{91} is not a direct determinant of USP12 nuclear export.

Importantly, it has been previously stated, as data not shown, that "NES" mutations prevent USP12 binding to UAF1 and WDR20 (Sanyal, 2016). Using co-IP analyses, we found that YFP-$USP12^{"NES"m}$ retained its ability to interact with Xpress-UAF1 (Fig. 6d, left). However "NES" mutations did efficiently disrupt the interaction of USP12 with Myc-WDR20 (Fig. 6d, right). The "NES" is located far away from the reported USP12/WDR20 interaction site (Li et al., 2016). It is likely that introducing six amino acid substitutions may result in non-specific changes in USP12 conformation that indirectly interfere with WDR20 binding. Importantly, by disrupting the interaction with WDR20, "NES" mutations abrogate WDR20-induced relocation of USP12 to the PM (Additional File 3), and would also prevent its full catalytic activation.

3.8. WDR20 bears a functional NES that mediates its CRM1-dependent nuclear export

The pronounced shift on the nucleocytoplasmic distribution of WDR20 caused by LMB prompted us to search for potential CRM1-dependent NESs in this protein. NESs usually adopt a characteristic secondary structure comprising an N-terminal alpha helix followed by a C-terminal loop (Dong et al., 2009). WDR20 does not present any alpha helical region according to the reported structure of the USP12/UAF1/WDR20 complex (Li et al., 2016). However, we noted that a WDR20 region comprising residues 394–509 was not solved in this structure. Thus, we decided to carry out a deletion analysis using three WDR20

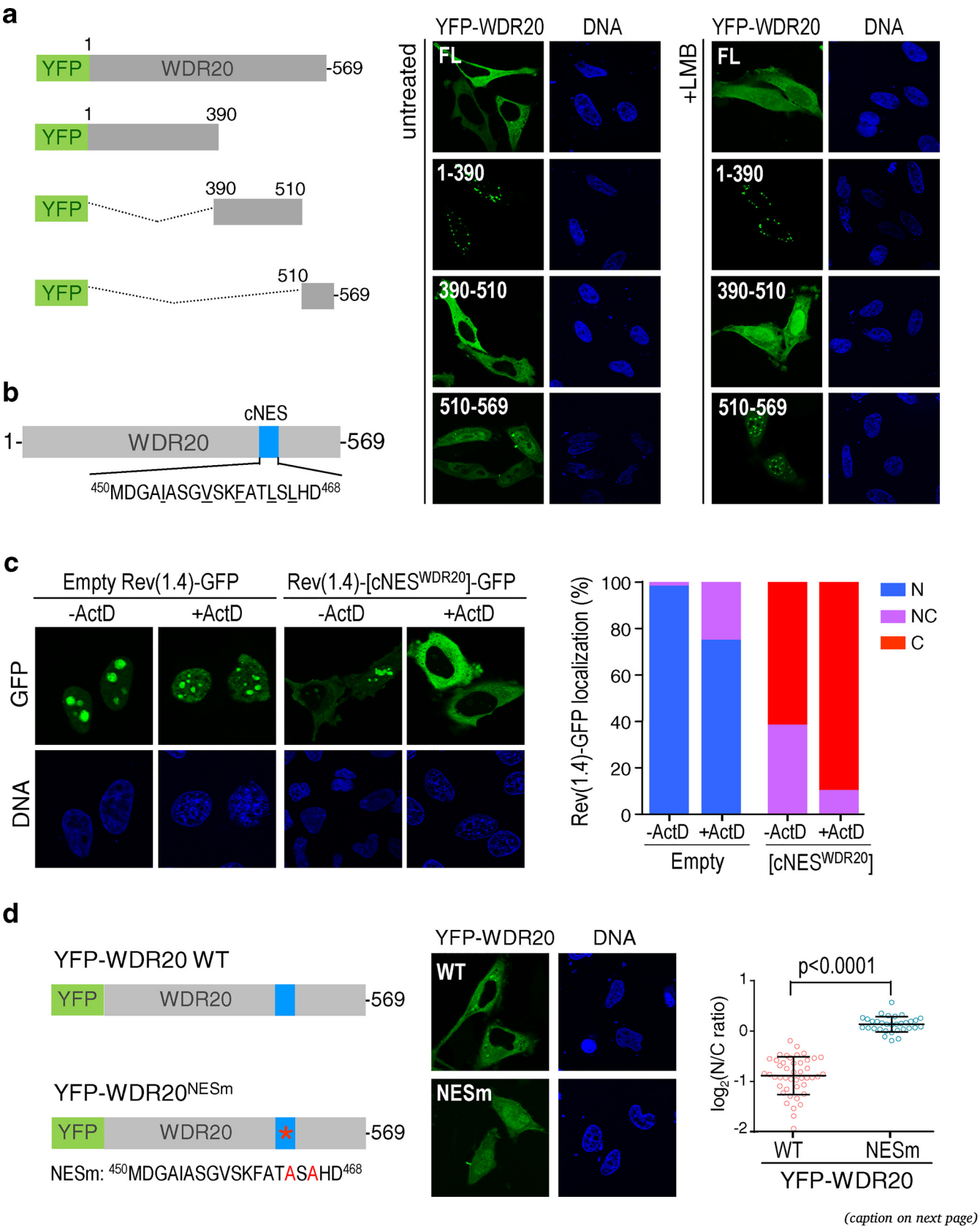

(caption on next page)

fragments: 1–390, 390–510 and 510-569. YFP-tagged versions of these fragments were expressed in HeLa cells, and their localization examined in the presence or absence of LMB (Fig. 7a). Like full-length YFP-WDR20, YFP-WDR20(390–510) clearly relocated from the cytoplasm to the nucleus in LMB-treated cells, suggesting that a CRM1-dependent NES may be located within this fragment. Using the NES prediction tool Wregex (Prieto et al., 2014), we found a candidate NES (cNES) motif (^{450}MDGAIASGVSKFATLSLHD^{468}) in this region (Fig. 7b), and tested it

Fig. 7. WDR20 bears a functional NES that mediates its CRM1-dependent nuclear export.
a. *Left*. Schematic representation of YFP-tagged WDR20 deletion mutants. *Right*. Confocal images of HeLa cells transfected with the different YFP-WDR20 deletion mutants and left untreated or treated with LMB (6 ng/ml for 3 h). LMB treatment induced relocation of full-length YFP-WDR20 and YFP-WDR20 (390–510) from the cytoplasm to the nucleus. **b**. Schematic representation of WDR20 protein showing the position and amino acid sequence of a candidate NES (cNES) predicted using the prediction webtool Wregex (Prieto et al., 2014). The hydrophobic residues that conform to the NES consensus are underlined. **c**. Results of a nuclear export assay to test the activity of the candidate WDR20 NES motif. *Left*. Confocal images showing representative examples of HeLa cells transfected with the empty Rev(1.4)-GFP plasmid or with the plasmid Rev(1.4)-[cNES^{WDR20}]-GFP, containing WDR20 candidate NES. *Right*. Graph showing the percentage of cells with mostly nuclear (N), nuclear and cytoplasmic (NC) or mostly cytoplasmic (C) localization of the reporter. At least 200 transfected cells were scored per condition. The WDR20 candidate NES motif readily promoted nuclear export of the Rev(1.4)-GFP reporter. **d**. *Left*. Schematic representation of wild type YFP-WDR20 and YFP-WDR20^{NESm}, a mutant bearing alanine substitutions of two NES residues (L464 and L466) (highlighted in red). *Center*. Representative examples of HeLa cells expressing YFP-WDR20 and YFP-WDR20^{NESm}. *Right*. Graph showing the N/C ratio of both proteins determined using image analysis of at least 30 transfected cells per sample. Each circle in the graph represents a single cell, and the mean (+/- SD) is shown. p value (Mann-Whitney U test) is indicated.

using the Rev(1.4)-GFP nuclear export assay. In contrast to USP12 "NES", WDR20 cNES efficiently promoted the export of the Rev(1.4)-GFP reporter to the cytoplasm (Fig. 7c), indicating that this motif constitutes a functional NES. Using the assay scoring system (Henderson and Eleftheriou, 2000), a score of 6+ was assigned to the WDR20 NES. Finally, we generated an NES-mutant version of YFP-WDR20 (YFP-WDR20^{NESm}) bearing mutations in two leucine residues (L464 A/L466 A). As shown in Fig. 7d, these mutations fully mimicked the effect of LMB treatment, confirming that the ^{450}MDGAIASGVSKF-ATLSLHD^{468} motif is a novel NES that mediates CRM1-dependent nuclear export of WDR20.

3.9. The CRM1 pathway and WDR20 NES mediate nucleocytoplasmic shuttling of the USP12/UAF1/WDR20 complex

In order to test the possibility that WDR20 NES regulates the localization of USP12 deubiquitinase complexes, 293 T cells were co-transfected with YFP-USP12$^{[+NLSs]}$ and either wild type or NES-mutant Myc-WDR20. As shown in Fig. 8a, YFP-USP12$^{[+NLSs]}$ located almost exclusively to the PM when co-expressed with wild type Myc-WDR20. In striking contrast, YFP-USP12$^{[+NLSs]}$ located to both the nucleus and the PM when co-expressed with Myc-WDR20^{NESm}, a distribution that was similar to that of YFP-USP12$^{[+NLSs]}$ co-expressed with wild type Myc-WDR20 after LMB treatment (see Fig. 5c). Of note, when a similar experiment was carried out using YFP-USP12 (without the added SV40 NLSs), both wild type and NES mutant Myc-WDR20 similarly co-localized with the DUB in the PM (Additional File 4a). This observation suggests that, in the absence of a strong NLS in USP12, recruitment to the PM largely prevails over slow diffusion into the nucleus upon formation of a USP12/WDR20 complex.

On the other hand, since YFP-USP46 was not recruited to the PM, but accumulated in the cytoplasm when co-expressed with Myc-WDR20 (see Fig. 2b), we tested the role of WDR20 NES on the localization of the USP46/WDR20 complex. Image analysis showed that the nuclear to cytoplasmic ratio of YFP-USP46 was significantly higher when expressed with Myc-WDR20^{NESm} than with wild type Myc-WDR20 (Additional File 4b), suggesting that the NES of WDR20 contributes to the cytoplasmic localization of the USP46/WDR20 complex.

Finally, triple co-transfection experiments were carried out to assess the role of the CRM1 pathway and WDR20 NES in the localization of the ternary USP12/UAF1/WDR20 complex. On one hand, 293 T cells were co-transfected with YFP-USP12$^{[+NLSs]}$, UAF1-mRFP, and wild type Myc-WDR20 and either left untreated or treated with LMB. On the other hand, cells were co-transfected with YFP-USP12$^{[+NLSs]}$, UAF1-mRFP and NES-mutant Myc-WDR20. As shown in Fig. 8b, LMB treatment or mutation of WDR20 NES resulted in a prominent relocation of the three co-expressed proteins to the nucleus. These findings strongly suggest the WDR20 NES described here mediates CRM1-dependent nuclear export of the USP12/UAF1/WDR20 complex.

4. Discussion

The mechanisms that regulate the subcellular localization of human deubiquitinating enzymes USP12 and USP46 have not been investigated in detail. Specifically, no attempts have been yet made to investigate potential differences between these very closely related DUBs in terms of their distribution inside the cell. The WDR proteins UAF1 and WDR20 have been well characterized as necessary cofactors that increase the catalytic activity of USP12 and USP46 (Cohn et al., 2009: Kee et al., 2010; Burska et al., 2013; Dahlberg and Juo, 2014; Li et al., 2016). UAF1, but not WDR20, is also a cofactor for the related DUB USP1 (Cohn et al., 2007). In this case, UAF1 plays a dual regulatory role, contributing not only to increase activity, but also to substrate recruitment (Lee et al., 2010; Yang et al., 2011). Here we show that WDR20 similarly plays a dual role in the regulation of USP12 and USP46. Besides increasing the activity of these enzymes, WDR20 contributes to modulate two aspects of their subcellular localization. On one hand, binding to WDR20 promotes relocation of USP12, but not USP46, to the plasma membrane (PM). On the other hand, WDR20 bears a nuclear export sequence (NES) that mediates CRM1-dependent nuclear export of WDR20-containing DUB complexes.

Contradictory findings regarding the subcellular localization of USP12 and USP46 have been previously reported in different cell types and using different experimental approaches (Joo et al., 2011; Urbé et al., 2012; Lehoux et al., 2014; Jahan et al., 2016). Here we have compared the distribution of USP12 and USP46 in 293 T and HeLa cells using epitope-tagged proteins. While we recognize that this approach may have limitations, our goal was to unequivocally assess the localization of each DUB. In this regard, it has been previously noted that the high similarity between USP12 and USP46 complicates the development of specific reagents to study the endogenous proteins (Joo et al., 2011).

In line with previous studies (Urbé et al., 2012; Lehoux et al., 2014), we found that YFP-USP12 and YFP-USP46 were located predominantly in the cytoplasm of 293 T and HeLa cells when expressed alone. In these conditions, ectopically expressed USP12 and USP46 would presumably be in excess over endogenous UAF1 and WDR20. Thus, we used double and triple co-transfections in an attempt to balance the expression levels of the complex subunits, and test a potential effect of the cofactors on the localization of the DUBs. The most striking finding was the relocation of YFP-USP12, but not YFP-USP46 to the PM when co-expressed with Myc-WDR20.

USP12 and USP46 are paralogs, evolved by duplication of a common ancestor gene (Vlasschaert et al., 2017), and the differential effect of WDR20 binding on their localization described here represents an example of evolutionary divergence, which correlates with the partial functional divergence exhibited by these enzymes. The yeast *S. pombe* encodes a single homologue of both human USP12 and USP46 (Ubp9), whose activity and localization is regulated by the yeast homologues of human UAF1 and WDR20 (Bun107 and Bun62) (Kouranti et al., 2010). Remarkably, while WDR protein-mediated catalytic activation of USP12 and USP46 has been conserved, these DUBs have evolved a striking difference in their ability to be recruited to the PM upon WDR20 binding. We have partially mapped this difference to a four amino-acid sequence (^{1}MEIL^{4}) present in USP12, but absent in USP46. We speculate that this motif could mediate transient

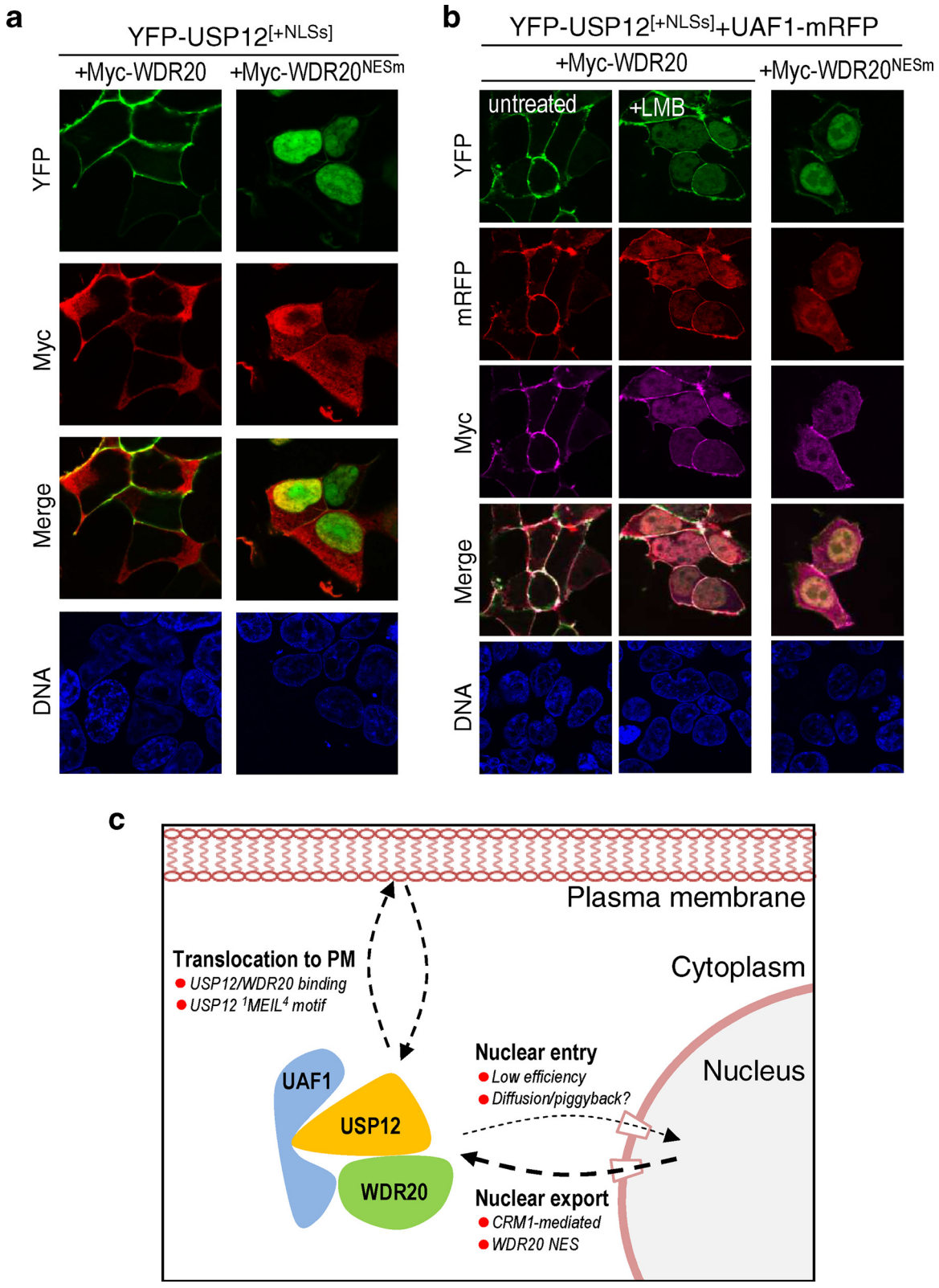

Fig. 8. The CRM1 pathway and WDR20 NES mediate nucleocytoplasmic shuttling of the USP12/UAF1/WDR20 complex.
a. Confocal images of 293 T cells co-expressing YFP-USP12$^{[+NLSs]}$ with either wild type Myc-WDR20 or Myc-WDR20^{NESm}. WDR20 NES mutation leads to accumulation of co-expressed YFP-USP12$^{[+NLSs]}$ and Myc-WDR20^{NESm} in the nucleus. **b**.Representative examples of the results of a triple co-transfection experiment in 293 T cells. On one hand, cells were co-transfected with YFP-USP12$^{[+NLSs]}$, UAF1-mRFP and wild type Myc-WDR20 and either left untreated or treated with LMB (6 ng/ml for 3 h). On the other hand, cells were co-transfected with YFP-USP12$^{[NLSs]}$, UAF1-mRFP and Myc-WDR20^{NESm}. In untreated cells, the ternary complex containing wild type WDR20 localizes almost exclusively to the PM. In contrast, the complex significantly accumulates in the nucleus when the CRM1 pathway is inhibited, or when it contains WDR20^{NESm}. **c**. A proposed model summarizing our results.

interactions of USP12 with still unidentified PM proteins or lipids. Since WDR20 binding induces a variety of rearrangements in USP12 structure (Li et al., 2016), it might promote PM recruitment by increasing the exposure of the ^{1}MEIL^{4} motif. Unfortunately, the currently available structure of the USP12/UAF1/WDR20 complex does not provide information on the extreme amino-terminal end of USP12. Further experiments should dissect the mechanisms by which WDR20 binding and the ^{1}MEIL^{4} motif contribute to the PM localization of USP12.

Besides uncovering the WDR20-promoted recruitment of USP12 to the PM, our data provide novel mechanistic insight into another closely related aspect of the subcellular localization of this DUB: its nucleocytoplasmic transport. We confirm that USP12 undergoes CRM1-dependent nuclear export in human cells, as described before (Jahan et al., 2016). In fact, our experiments indicate that both USP12 and WDR20 relocate from the cytoplasm to the nucleus when CRM1 is inhibited with LMB.

Importantly, neither USP12 nor WDR20 accumulate to high levels in the nucleus of LMB-treated cells, suggesting that they are not efficiently imported into the nucleus, probably due to the lack of active NLSs. In support of this view, we show that fusing two copies of the SV40 large T antigen NLS to YFP-USP12 readily induces its nuclear accumulation. We suggest that endogenous USP12 complexes may enter the nucleus by diffusion or by using a piggyback mechanism. In fact, an example of piggyback nuclear import of USP12 and USP46 mediated by the human papillomavirus E1 protein has been already described (Lehoux et al., 2014). Remarkably, we found that the variant of USP12 carrying strong heterologous NLSs (YFP-USP12$^{[+NLSs]}$) was exclusively located to the PM when co-expressed with Myc-WDR20, but partially relocated to the nucleus upon LMB treatment, suggesting that the YFP-USP12$^{[+NLSs]}$/Myc-WDR20 complex is in fact continuously shuttling between the PM, cytoplasm and nucleus in a CRM1-dependent manner.

Studies on yeast and human cells (Kouranti et al., 2010; Jahan et al., 2016) demonstrate that CRM1-dependent shuttling is an evolutionarily conserved, and thus probably important, feature of USP12 complexes, whose details remain poorly characterized. We provide novel mechanistic insight into the nucleocytoplasmic transport of USP12 complexes.

First, our data suggest that a previously reported USP12 “NES” (^{77}KESLLTCLADLFHSI^{91}) (Jahan et al., 2016; Sanyal, 2016) is not a direct determinant of CRM1-dependent export. This motif was non-functional in a nuclear export assay (Henderson and Eleftheriou, 2000), and mutations of this “NES” (unlike LMB treatment) did not decrease the cytoplasmic localization of YFP-USP12 in HeLa cells. In the previous report (Jahan et al., 2016), the localization of USP12 was determined in Jurkat cells using a fractionation protocol based on permeabilization of the PM to separate soluble (cytosolic) and pellet (nuclear) fractions. “NES” mutations were reported to prevent USP12 translocation to the cytosol, and to abrogate USP12-mediated stabilization of the T-cell receptor complex (Jahan et al., 2016). Importantly, it was pointed out (as data not shown) that “NES” mutations abrogate USP12 interaction with UAF1 and WDR20 (Sanyal, 2016). We confirmed that “NES” mutations disrupt USP12/WDR20 interaction. In the light of the novel evidence presented here, we believe that several conclusions from the previous report (Jahan et al., 2016) should be reconsidered. On one hand, it should be taken into account that their pellet fractions might contain PM-located as well as nuclear USP12. More importantly, since “NES” mutations disrupt WDR20 binding, the reported functional abrogation of “NES”-mutant USP12 (Jahan et al., 2016) might be related to incomplete catalytic activation of the enzyme rather than to altered nuclear export.

Second, we have identified a *bona fide* novel NES in WDR20. The WDR20 motif ^{450}MDGAIASGVSKFATLSLHD^{468} was clearly functional in the nuclear export assay, and mutation of this sequence caused a partial relocation of epitope-tagged WDR20 from the cytoplasm to the nucleus, mimicking the effect of LMB.

Finally, we show that mutation of WDR20 NES interferes with the nuclear export of USP12/WDR20 and USP12/UAF1/WDR20 complexes. Of note, we used the YFP-USP12$^{[+NLSs]}$ variant in these experiments as a tool to more clearly visualize the effect of WDR20 NES mutations. Although the WDR20 region containing the NES is not solved in the currently available structure of the USP12/UAF1/WDR20 complex, these results suggest that the WDR20 NES is accessible for CRM1 interaction in the context of the ternary complex.

The dynamic shuttling of USP12 complexes described here may facilitate access of this DUB to nuclear substrates such as histones (Joo et al., 2011), as well as to substrates that are located in the cytoplasm and the PM, such as PHLPP (Gangula and Maddika, 2013; Li et al., 2013). Our results are based on co-overexpression experiments to achieve balanced levels of the different subunits, and formation of different subcomplexes of USP12, UAF1 and WDR20. Although it is presently unclear if these different subcomplexes exist physiologically in the cell, we speculate that at endogenous (lower) levels of all subunits, those USP12 subcomplexes that contain WDR20 would be predominantly located to the PM. Thus, our data suggest that USP12 subcomplexes with different stoichiometry might not only have different level of catalytic activity, as it would be expected from previous results (Cohn et al., 2009; Kee et al., 2010; Kouranti et al., 2010; Burska et al., 2013; Dahlberg and Juo, 2014; Li et al., 2016) but they might also localize to different subcellular compartments. Mechanisms that may modulate WDR20 localization, such as post-translational modification, might in turn modulate the localization of DUB complexes containing this subunit.

5. Conclusions

Our results support a model (Fig. 8c) whereby the USP12/UAF1/WDR20 complex has the ability to dynamically shuttle between the PM cytoplasm and nucleus. WDR20 plays a crucial role in this shuttling as a “targeting subunit” of the complex. On one hand, its direct binding to USP12 would promote transient recruitment to the PM and, on the other hand, its NES would mediate CRM1-dependent nuclear export.

Authors´ contributions

AO-H designed and carried out experiments, and contributed to writing the manuscript. MS designed and carried out experiments. IA-C developed experimental tools. JAR conceived the study, designed experiments and contributed to writing the manuscript. All authors read and approved the final manuscript.

Funding

This work was supported by grants from the Spanish Government MINECO-FEDER (SAF2014-57743-R), the Basque Country Government (IT634-13) and the University of the Basque Country (UFI11/20), as well as fellowships from the Basque Country Government (to MS) and the University of the Basque Country (to AO-H). Our group is a member of the PROTEOSTASIS BM1307 COST Action, supported by European Cooperation in Science and Technology.

Competing interests

The authors declare that they have no competing interests.

Acknowledgements

We appreciate the generous gift of plasmids from Dr. René Bernards, Dr. Jae Jung and Dr. Beric Henderson. We appreciate the technical support by the staff from the High Resolution Microscopy Facility (SGIKER-UPV/EHU).

Appendix A. Supplementary data

Supplementary material related to this article can be found, in the online version, at doi:https://doi.org/10.1016/j.ejcb.2018.10.003.

References

Bardwell, L., 2006. Mechanisms of MAPK signalling specificity. Biochem. Soc. Trans. 34 (5), 837–841.

Burska, U.L., Harle, V.J., Coffey, K., Darby, S., Ramsey, H., O´Neill, D., et al., 2013. Deubiquitinating enzyme Usp12 is a novel co-activator of the androgen receptor. J. Biol. Chem. 288, 32641–32650.

Cohn, M.A., Kowal, P., Yang, K., Haas, W., Huang, T.T., Gygi, S.P., et al., 2007. A UAF1-containing multisubunit protein complex regulates the Fanconi anemia pathway. Mol. Cell 28, 786–797.

Cohn, M.A., Kee, Y., Haas, W., Gygi, S.P., D´Andrea, A.D., 2009. UAF1 is a subunit of multiple deubiquitinating enzyme complexes. J. Biol. Chem. 284, 5343–5351.

Dahlberg, C.L., Juo, P., 2014. The WD40-repeat proteins WDR-20 and WDR-48 bind and activate the deubiquitinating enzyme USP-46 to promote the abundance of the glutamate receptor GLR-1 in the ventral nerve cord of Caenorhabditis elegans. J. Biol. Chem. 289, 3444–3456.

Dharadhar, S., Clerici, M., van Dijk, W.J., Fish, A., Sixma, T.K., 2016. A conserved two-step binding for the UAF1 regulator to the USP12 deubiquitinating enzyme. J. Struct. Biol. 196, 437–447.

Dong, X., Biswas, A., Süel, K.E., Jackson, L.K., Martinez, R., Gu, H., et al., 2009. Structural basis for leucine-rich nuclear export signal recognition by CRM1. Nature 458 (7242), 1136–1141.

Fraile, J.M., Quesada, V., Rodríguez, D., Freije, J.M.P., López-Otín, C., 2012. Deubiquitinases in cancer: new functions and therapeutic options. Oncogene 31, 2373–2388.

Gangula, N.R., Maddika, S., 2013. WD repeat protein WDR48 in complex with deubiquitinase USP12 suppresses Akt-dependent cell survival signalling by stabilizing PH domain leucine-rich repeat protein phosphatise 1 (PHLPP1). J. Biol. Chem. 288, 34545–34554.

Haahr, P., Borgermann, N., Guo, X., Typas, D., Achuthankutty, D., Hoffmann, S., et al., 2018. ZUFSP deubiquitylates K63-linked polyubiquitin chains to promote genome stability. Mol. Cell 70 (1), 165–174.

Huo, Y., Khatri, N., Hou, Q., Gilbert, J., Wang, G., Man, H.Y., 2015. The deubiquiting enzyme USP46 regulates AMPA receptor ubiquitination and trafficking. J. Neurochem. 134 (6), 1067–1080.

Jahan, A.S., Lestra, M., Swee, L.K., Fan, Y., Lamers, M.M., Tafesse, F.G., et al., 2016. Usp12 stabilizes the T-cell receptor complex at the cell surface during signalling. Proc. Natl. Acad. Sci. U. S. A. 113 (6), E705–714.

Joo, H.Y., Jones, A., Yang, C., Zhai, L., Smith, A.D., Zhang, Z., et al., 2011. Regulation of histone H2A and H2B deubiquitination and Xenopus development by USP12 and USP46. J. Biol. Chem. 286, 7190–7201.

Kee, Y., Yang, K., Cohn, M.A., Haas, W., Gygi, S.P., D´Andrea, A.D., 2010. WDR20 regulates activity of the USP12-UAF1 deubiquitinating enzyme complex. J. Biol. Chem. 285, 11252–11257.

Komander, D., Clague, M.J., Urbé, S., 2009. Breaking the chains: structure and function of the deubiquitinases. Nat. Rev. Mol. Cell Biol. 10 (8), 550–563.

Kouranti, I., McLean, J.R., Feoktistova, A., Liang, P., Johnson, A.E., Roberts-Galbraith, R.H., et al., 2010. A global census of fission yeast deubiquitinating enzyme localization and interaction networks reveals distinct compartmentalization profiles and overlapping functions in endocytosis and polarity. PLoS Biol. https://doi.org/10.1371/journal.pbio.1000471.

Kwasna, D., Rehman, Abdul, SA, Natarajan, J., Matthews, S., Madden, R., De Ce sare, V., et al., 2018. Discovery and Characterization of ZUFSP/ZUP1, a distinct deubiquitinase class important for genome stability. Mol. Cell 70 (1), 150–164.

Lee, K.Y., Yang, K., Cohn, M.A., Sikdar, N., D´Andrea, A.D., Myung, K., 2010. Human ELG1 regulates the level of ubiquitinated proliferating cell nuclear antigen (PCNA) through its interactions with PCNA and USP1. J. Biol. Chem. 285 (14), 10362–10369.

Legland, D., Arganda-Carreras, I., Andrey, P., 2016. MorphoLibJ: integrated library and plugins for mathematical morphology with ImageJ. Bioinformatics 32 (22), 3532–3534.

Lehoux, M., Gagnon, D., Archambault, J., 2014. E1-mediated recruitment of a UAF1-USP deubiquitinase complex facilitates human papillomavirus DNA replication. J. Virol. 88 (15), 8545–8555.

Li, X., Stevens, P.D., Yang, H., Gulhati, P., Wang, W., Evers, B.M., et al., 2013. The deubiquitination enzyme USP46 functions as a tumor suppressor by controlling PHLPP-dependent attenuation of Akt signalling in colon cancer. Oncogene 32, 471–478.

Li, H., Lim, K.S., Kim, H., Hinds, T.R., Jo, U., Mao, H., et al., 2016. Allosteric activation of ubiquitin-specific proteases by β-propeller proteins UAF1 and WDR20. Mol. Cell 6, 249–260.

Manning, B.D., Toker, A., 2017. AKT/PKB signalling: navigating the network. Cell 169 (3), 381–405.

McClurg, U.L., Summerscales, E.E., Harle, V.J., Gaughan, L., Robson, C.N., 2014. Deubiquitinating enzyme Usp12 regulates the interaction between the androgen receptor and the Akt pathway. Oncotarget 5, 7081–7092.

McClurg, U.L., Harle, V.J., Nabbi, A., Batalha-Pereira, A., Walker, S., Coffey, K., et al., 2015. Ubiquitin-specific protease 12 interacting parterns Uaf-1 and WDR20 are potential therapeutic targets in prostate cancer. Oncotarget 6 (35), 37724–37736.

Mevissen, T.E.T., Komander, D., 2017. Mechanisms of deubiquitinase specificity and regulation. Annu. Rev. Biochem. 86, 159–192.

Moretti, J., Chastagner, P., Liang, C.C., Cohn, M.A., Israël, A., Brou, C., 2012. The ubiquitin-specific protease 12 (USP12) is a negative regulator of notch signaling acting on notch receptor trafficking toward degradation. J. Biol. Chem. 287, 2006–2016.

Olazabal-Herrero, A., García-Santisteban, I., Rodriguez, J.A., 2015. Structure-function analisis of USP1: insights into the role of Ser313 phosphorylation site and the effect of cancer-associated mutations on autocleavage. Mol. Cancer. https://doi.org/10.1186/s12943-015-0311-7.

Prieto, G., Fullaondo, A., Rodriguez, J.A., 2014. Prediction of nuclear export signals using weighted regular expressions (Wregex). Bioinformatics 30 (9), 1220–1227.

Sanyal, S., 2016. Reply to Rodriguez: mechanism of nuclear-cytosol chuttling of Usp12. Proc. Natl. Acad. Sci. U. S. A. 113 (24), E3317–3318.

Schindelin, J., Arganda-Carreras, I., Frise, E., Kaynig, V., Longair, M., Pietzsch, T., 2012. Fiji: an open-source platform for biological-image analysis. Nat. Methods 9 (7), 676–682.

Sowa, M.E., Bennett, E.J., Gygi, S.P., Harper, J.W., 2009. Defining the human deubiquitinating enzyme interaction landscape. Cell 138, 389–403.

Urbé, S., Liu, H., Hayes, S.D., Heride, C., Rigden, D.J., Clague, M.J., 2012. Systematic survey of deubiquitinase localization identifies USP21 as a regulator of centrosome- and microtubule-associated functions. Mol. Biol. Cell 23, 1095–1103.

Vlasschaert, C., Cook, D., Xia, X., Gray, D.A., 2017. The evolution and functional diversification of the deubiquitinating enzyme superfamily. Genome Biol. Evol. 9 (3), 558–573.

Wei, R., Liu, X., Yu, W., Yang, T., Cai, W., Liu, J., et al., 2015. Deubiquitinases in cancer. Oncotarget 6 (15), 12872–12889.

Yang, K., Moldovan, G.L., Vinciguerra, P., Murai, J., Takeda, S., D´Andrea, A.D., 2011. Regulation of the Fanconi anemia pathway by a SUMO-like delivery network. Genes Dev. 25, 1847–1858.

Ye, Y., Scheel, H., Hofmann, K., Komander, D., 2009. Dissection of USP catalytic domains reveals five common insertion points. Mol. Biosyst. 5 1979-1808.

Yin, J., Schoeffler, A.J., Wickliffe, K., Newton, K., Starovasnik, M.A., Dueber, E.C., et al., 2015. Structural insights into WD-repeat 48 activation of ubiquitin-specific protease 46. Structure 23 (11), 2043–2054.